World Journal of Advanced Research and Reviews
eISSN: 2581-9615 CODEN (USA): WJARAI
Cross Ref DOI: 10.30574/wjarr
Journal homepage: https://wjarr.com/

(Research Article)

Check for updates

DIFFUSION COEFFICIENT, CHARGE-CARRIER DENSITY, PHOTOCURRENT AND PHOTOVOLTAGE OF A PARALLEL VERTICAL-JUNCTION POLYCRYSTALLINE SILICON SOLAR CELL: COUPLED EFFECTS OF FREQUENCY, GRAIN BOUNDARIES AND GRAIN SIZE

Marcel Sitor Diouf *, Oulimata Mballo and Amary Thiam

Laboratory of Semiconductors and Solar Energy, Department of Physics, Faculty of Sciences and Techniques, Cheikh Anta Diop University (UCAD), Dakar, Senegal.
* Corresponding Author; E-mail: marceldiouf39@yahoo.fr

ORCID Details
Marcel Sitor Diouf: https://orcid.org/0009-0006-2806-3128

World Journal of Advanced Research and Reviews, 2026, 31(02), 1666–1669

Publication history: Received on 19 July 2026; revised on 27 August 2026; accepted on 29 August 2026

Article DOI: https://doi.org/10.30574/wjarr.2026.31.2.2232

ABSTRACT

In this work, we present a theoretical study of the combined effect of the modulation frequency (ω), the grain-boundary recombination velocity (Sg) and the grain size (g) on the fundamental transport parameters of a parallel vertical-junction polycrystalline silicon solar cell, namely the effective diffusion coefficient, the minority-carrier density, the photocurrent and the photovoltage. Solving the three-dimensional continuity equation by decomposition into a double Fourier series yields the expressions of these four quantities. Bode and Nyquist diagrams are used to analyse their behaviour. The main result of this work is the identification of a high-frequency convergence regime (beyond $\omega \approx 10^6$ rad/s), not previously reported in the literature on polycrystalline solar cells, in which all transport quantities converge toward values set by Sg and g. In this regime the dynamic diffusion length becomes too short for the carriers to reach the grain boundaries before the field reverses, opening the way to dynamic-regime operation as a strategy for partially circumventing microstructural limitations. A second, equally original result emerges from the direct comparison of the short-circuit photocurrent, the open-circuit voltage and the effective diffusion coefficient for the same set of microstructures: whereas D_eff varies by a factor greater than 10 depending on grain-boundary quality, Jsc varies by a factor smaller than 1.25 over the same range. This differential sensitivity reveals that the short-circuit current is a far less discriminating indicator of microstructural quality than base transport or the photogenerated voltage — an observation not formulated in this form in earlier studies of this type of structure.

Keywords: Vertical junction; Grain boundaries; Frequency domain; Effective diffusion coefficient; Photocurrent; Photovoltage.

1 INTRODUCTION

Photovoltaic conversion remains one of the most promising routes to meet the global energy demand, and polycrystalline silicon represents a favoured techno-economic compromise relative to monocrystalline silicon on account of its lower fabrication cost. This economic advantage is, however, accompanied by a major physical limitation: the presence of grain boundaries, which introduce additional recombination centres and degrade the cell performance relative to an ideal single-crystal material.

The effect of grain boundaries on the performance of polycrystalline solar cells has been studied since the 1980s by several reference authors, who established the founding models describing grain-boundary recombination and its impact on the short-circuit current and the open-circuit voltage [1–3]. These founding works are, however, restricted to the static regime and do not consider the dynamic response of the cell to a frequency-modulated excitation.

More recently, accounting for the dynamic frequency regime has made it possible to explore the capacitive response and the impedance of vertical-junction solar cells [4,5], revealing a low-pass behaviour and characteristic Bode and Nyquist diagrams. These studies focus, however, on single-crystal structures and do not address the interplay between frequency effects and grain boundaries. Conversely, three-dimensional modelling of grain-size effects and grain-boundary recombination has been treated in detail by Sene et al. [6], but only within the static regime. Three-dimensional models of polycrystalline cells under external fields have also been developed [7,8], as well as frequency-domain formulations of the diffusion coefficient and its equivalent-circuit representation [9]; vertical-junction architectures, for their part, have mostly been optimised in the static regime [10,11].

This study highlights the fact that the existing literature treats the effects of grain boundaries and of the modulation frequency separately. The present work aims to fill this gap for four fundamental transport parameters: the effective diffusion coefficient, the carrier density, the photocurrent and the photovoltage. The originality of the study rests on two major contributions.

First, the formulation of a coupled effective diffusion coefficient, relating the angular frequency ω to the eigenvalues associated with the grain boundaries, reveals a high-frequency convergence toward the intrinsic value of the material, independent of Sg and g; to our knowledge this result has not been reported in earlier studies of such structures.

Second, a direct comparison of the short-circuit current (Jsc), the open-circuit voltage (Voc) and the effective diffusion coefficient (D_eff) for the same set of microstructures reveals marked differences in sensitivity between these parameters. This suggests that relying solely on the short-circuit current, although it is the most common experimental characterisation measure, leads to a significant underestimation of the actual impact of microstructural quality on the transport of photogenerated minority carriers.

2 THEORY

The model considers an n-p-n parallel vertical-junction polycrystalline silicon solar cell whose base, of thickness gz, is structured into grains of size g. The structure of this solar cell is shown in Figure 1.

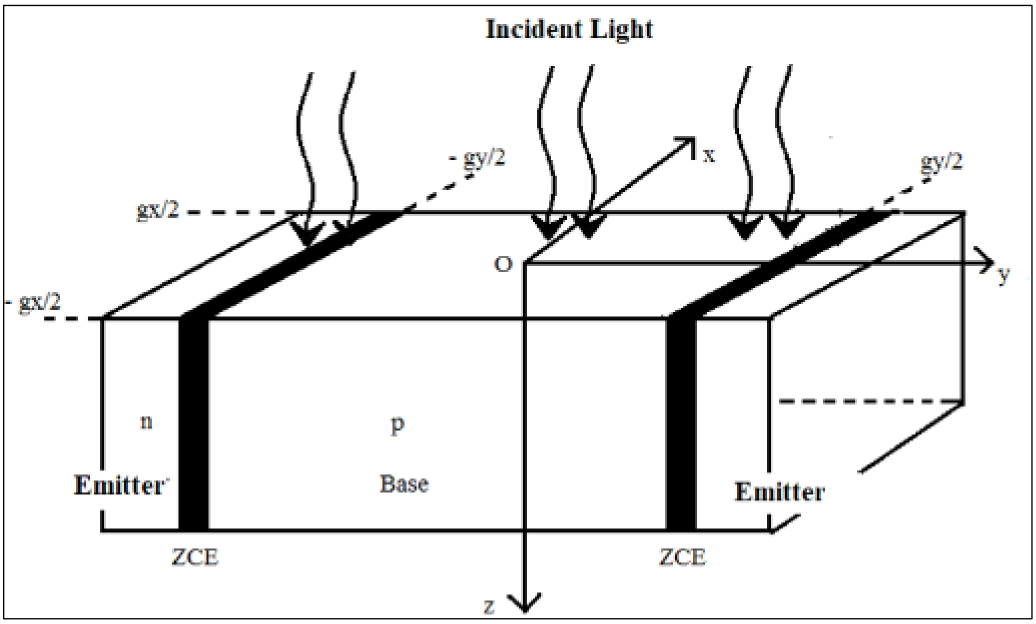

Figure 1: Three-dimensional structure of the vertical-junction solar cell.

A parallel vertical-junction solar cell consists of a set of cells whose bases are connected together and whose emitters are connected together. The structure of this solar cell is shown in Figure 2:

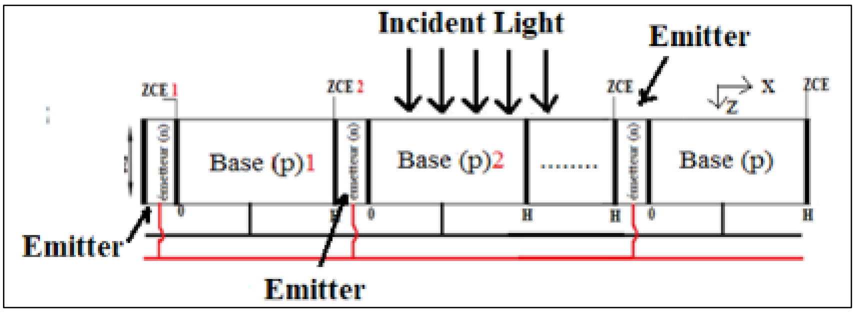

Figure 2: Parallel connection of the vertical-junction solar cell.

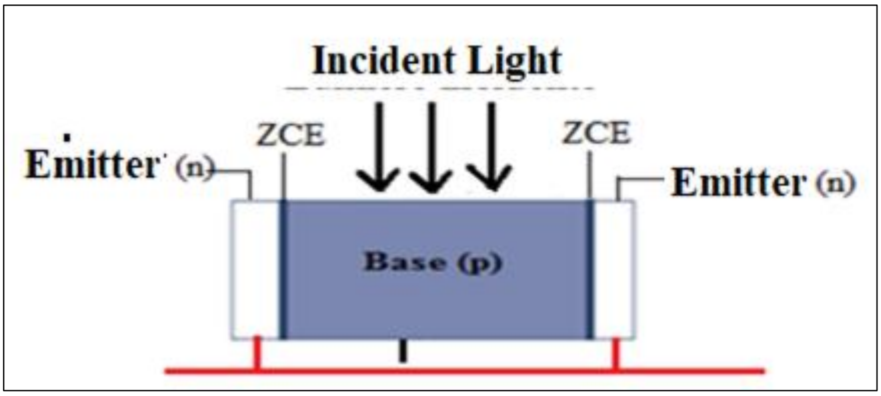

Figure 3: n-p-n vertical-junction solar cell.

Under frequency-modulated monochromatic illumination, the photogenerated minority-carrier density δn(x,y,z,t) obeys the three-dimensional continuity equation:

$$D.\nabla^2\delta n(x,y,z,t) - \frac{\delta n(x,y,z,t)}{\tau} + G(z,t) = \frac{\partial}{\partial t}\delta n(x,y,z,t) \qquad (1)$$

where D and τ are respectively the diffusion coefficient and the lifetime of the minority carriers in the grain, and g(z) is the generation rate. The mobility that sets the diffusion coefficient D follows the Arora model [12], and the depth-dependent generation rate g(z) follows the three-exponential Furlan–Amon approximation [13].

In the dynamic regime, the solution is expressed as a double Fourier series:

$$\delta n(x,y,z) = \sum_k \sum_j \left[A_1(k,j).\cosh\left(\frac{y}{L_{kj}}\right) + \left(\frac{\alpha(1-Rt)\varphi}{D_{kj}}\right).L_{kj}{}^2\right].\cos(Ck.x).\cos(Ej.z) \quad (2)$$

The coefficient A_1(k,j), determined by the recombination condition at the junction (velocity Sf), is given by:

$$A_1(k,j) = -\frac{Sf}{D}.L_{kj}{}^2.\frac{\frac{\alpha(1-Rt).\varphi}{D_{kj}}}{\frac{1}{L_{kj}}.\sinh\left(\frac{gy}{2.L_{kj}}\right)+\frac{Sf}{D}.cosh\left(\frac{gy}{2.L_{kj}}\right)} \quad (3)$$

The eigenvalues Ck (grain boundaries) and Ej (back surface) are the solutions of the transcendental equations, respectively:

$$\tan\left(\frac{Ck.g}{2}\right) = \frac{Sg}{Ck.D} \quad (4)$$

$$\tan(Ej.gz) = \frac{Sar}{Ej.D} \quad (5)$$

The dynamic diffusion length of the material and that of the (k,j) mode are given by:

$$Ln(\omega)^2 = \frac{L^2}{1+i\omega\tau} \quad (6)$$

$$L_{kj}(\omega)^2 = \frac{Ln(\omega)^2}{[1+Ln(\omega)^2.(Ej^2+Ck^2)]} \quad (7)$$

The effective diffusion coefficient of the fundamental mode (k=0, j=0), which accounts for the coupled effect of ω, Sg and g on transport, is defined by:

$$D_{-eff(\omega,Sg,g)} = \frac{D.L_{00}(\omega,Sg,g)^2}{Ln(\omega)^2} \quad (8)$$

From the density (2), the photocurrent and the photovoltage are obtained by integration at the junction (y = gy/2):

$$Jph = \frac{2.q.D}{g.gz}.\sum_k \sum_j \left[\frac{1}{Ck.Ej}.A_1.\frac{1}{L_{kj}}.sinh\left(\frac{gy}{2.L_{kj}}\right).sin\left(\frac{Ck.g}{2}\right).\sin(Ej.gz)\right] \quad (9)$$

$$Vph = Vt.\ln\left[1+\frac{2Nb}{Ni^2}.\sum\right] \quad (10)$$

with:

where q is the elementary charge, Vt the thermal voltage, Nb the base doping concentration and ni the intrinsic carrier concentration in silicon.

3 RESULTS AND DISCUSSION

3.1 Effective diffusion coefficient D_eff

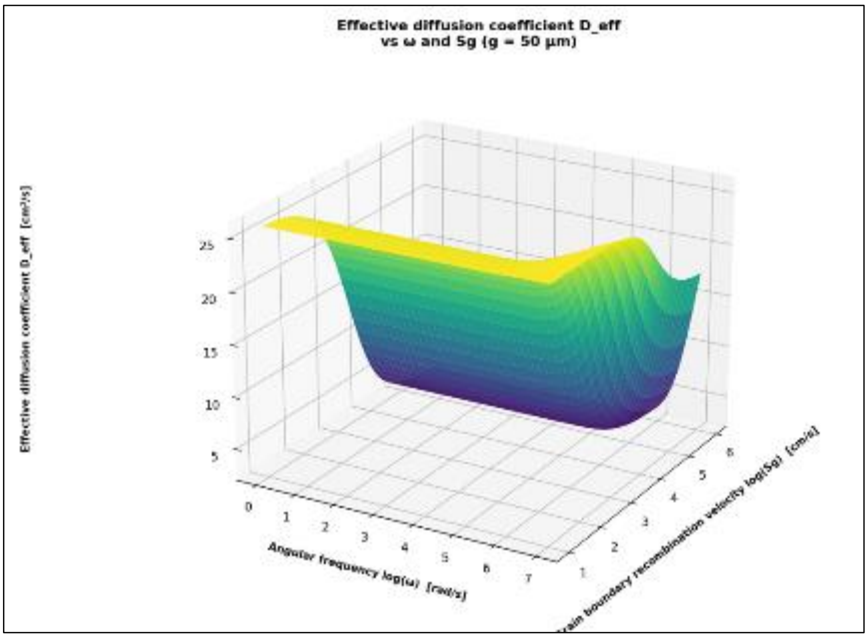

Figure 4: Effective diffusion coefficient D_eff as a function of the angular frequency ω and the grain-boundary recombination velocity Sg (g = 50 µm).

Figure 4 illustrates the effect of Sg for a given grain size: the low-frequency plateau of D_eff drops sharply as Sg increases, falling from about 25 cm^2/s at Sg = 10^2 cm/s to less than 3 cm^2/s at Sg = 10^6 cm/s — a degradation of more than one order of magnitude that highlights the direct sensitivity of minority-carrier transport in the base to grain-boundary quality. Beyond $\omega \approx 10^6$ rad/s, this dependence on Sg gradually weakens, all curves converging toward the value D = 26 cm^2/s.

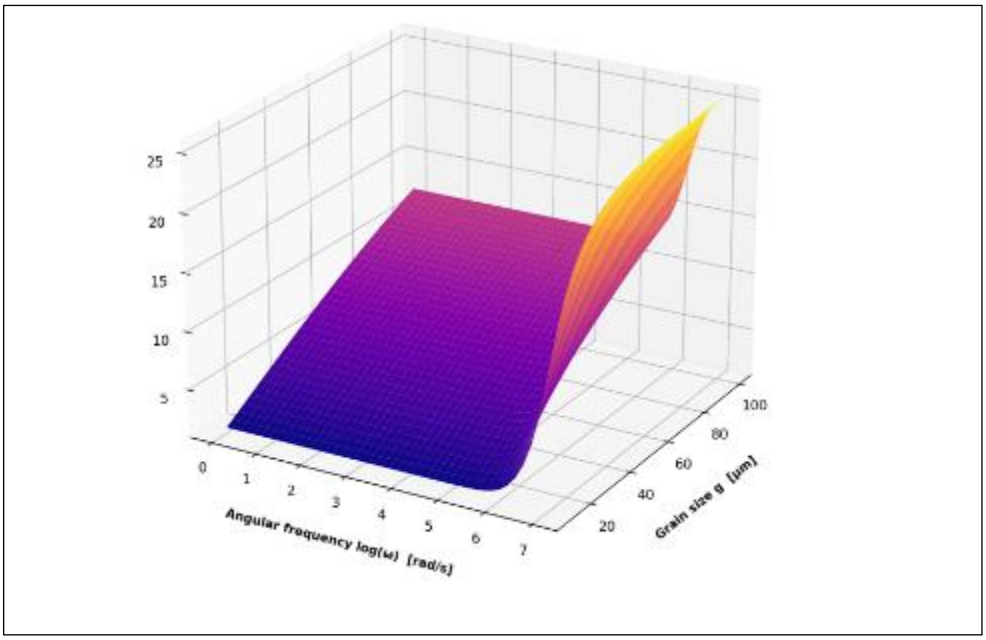

Figure 5: Effective diffusion coefficient D_eff as a function of the angular frequency ω and the grain size g (Sg = 10^4 cm/s).

Figure 5 isolates more precisely the effect of grain size: for a fixed Sg, the low-frequency plateau of D_eff increases continuously with g, rising from about 3 cm^2/s for small grains to more than 25 cm^2/s for large grains, close to the actual value D = 26 cm^2/s. Notably, the convergence frequency ($\approx 10^6$ rad/s) remains essentially the same regardless of grain size, indicating that this threshold is governed mainly by the induced material dynamics (τ) rather than by the microstructure itself.

These two behaviours thus converge to a common point beyond $\omega \approx 10^6$ rad/s: whatever the values of Sg and g, D_eff tends toward D = 26 cm^2/s, because the dynamic diffusion length becomes too short for the carriers to reach the grain boundaries before the field reverses, so that the boundaries no longer influence transport.

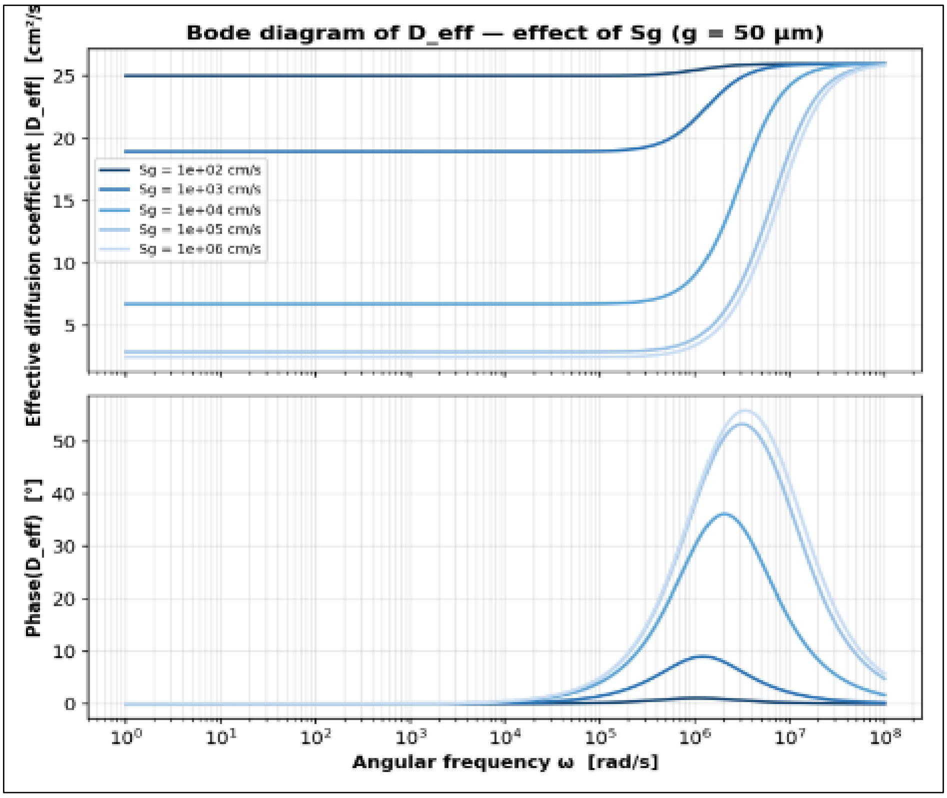

Figure 6: Bode diagram of the effective diffusion coefficient D_eff — effect of Sg (g = 50 µm).

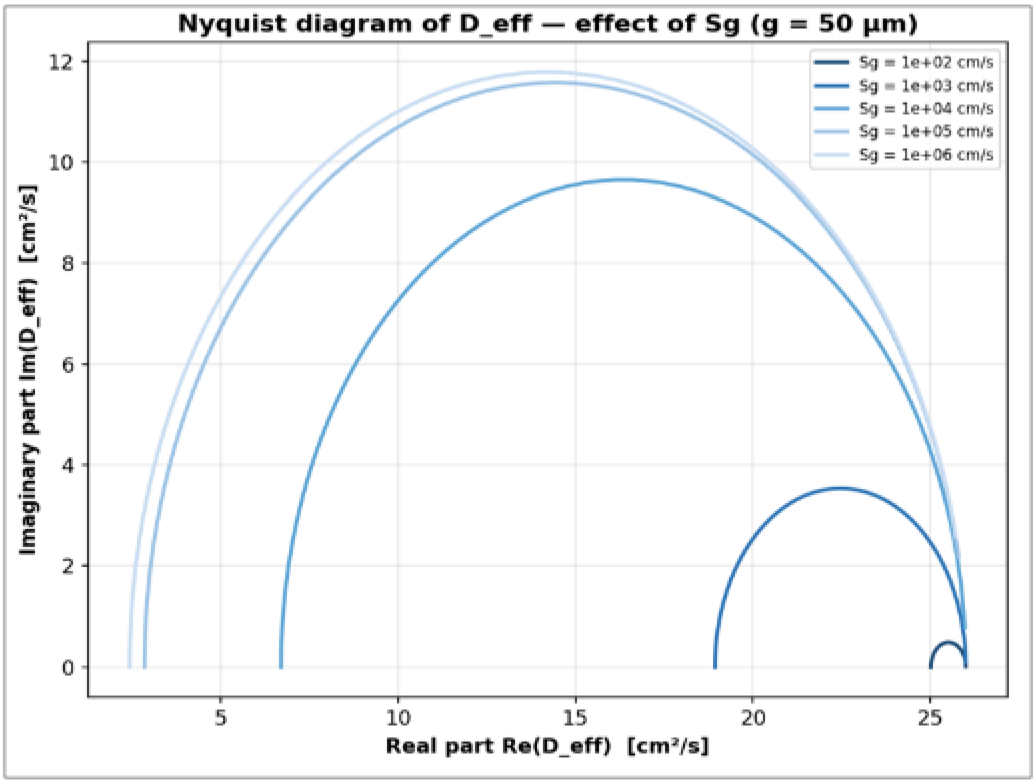

Figure 7: Nyquist diagram of the effective diffusion coefficient D_eff — effect of Sg (g = 50 µm).

The Bode diagrams confirm this low-frequency plateau and the high-frequency rise. The Nyquist diagrams show closed semicircular arcs, characteristic of a system with a single dominant time constant, whose diameter increases with Sg.

3.2 Minority-carrier density δn

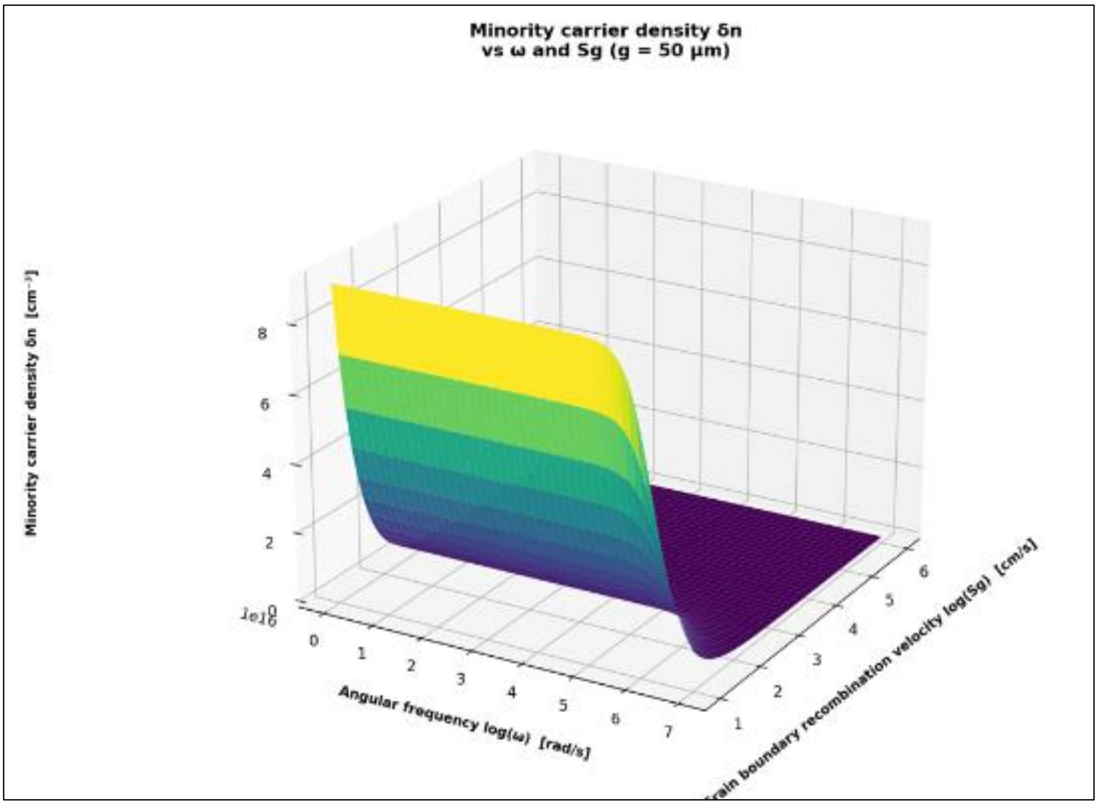

Figure 8: Minority-carrier density δn as a function of the angular frequency ω and the grain-boundary recombination velocity Sg (g = 50 µm).

The stored-carrier density reaches its maximum plateau (≈ 8×10^{12} cm^{-3} under the reference conditions) at low Sg, where grain-boundary recombination remains limited. As Sg increases, this plateau drops rapidly by nearly an order of magnitude, reflecting the progressive loss of carriers trapped by the grain boundaries before they can contribute to the density stored in the bulk.

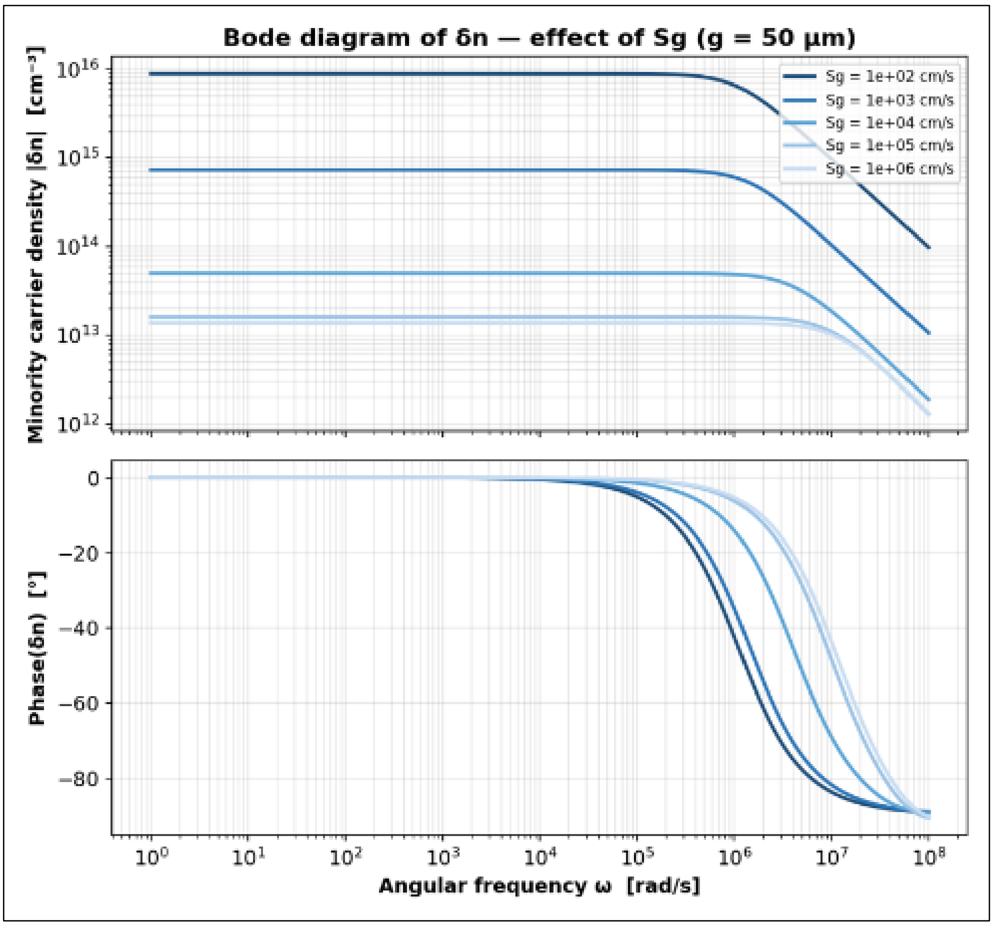

Figure 9: Bode diagram of the minority-carrier density δn — effect of Sg (g = 50 µm).

The Bode diagrams confirm this same low-pass behaviour: a constant plateau at low frequency and a decay beyond a cut-off frequency of the order of 10^5–10^6 rad/s. The normalised Nyquist diagrams (not shown here, but of a form similar to those of D_eff) indicate that the relaxation dynamics are almost independent of Sg and g, which affect only the amplitude of the stored density.

3.3 Photocurrent Jph

The photocurrent shows a clear separation of the curves with Sg at low frequency, with a maximum spread of about 25 % between the extreme Sg values studied — a narrow range that confirms, as observed in Table 1, the low relative sensitivity of Jph to grain-boundary quality compared with D_eff or Vph.

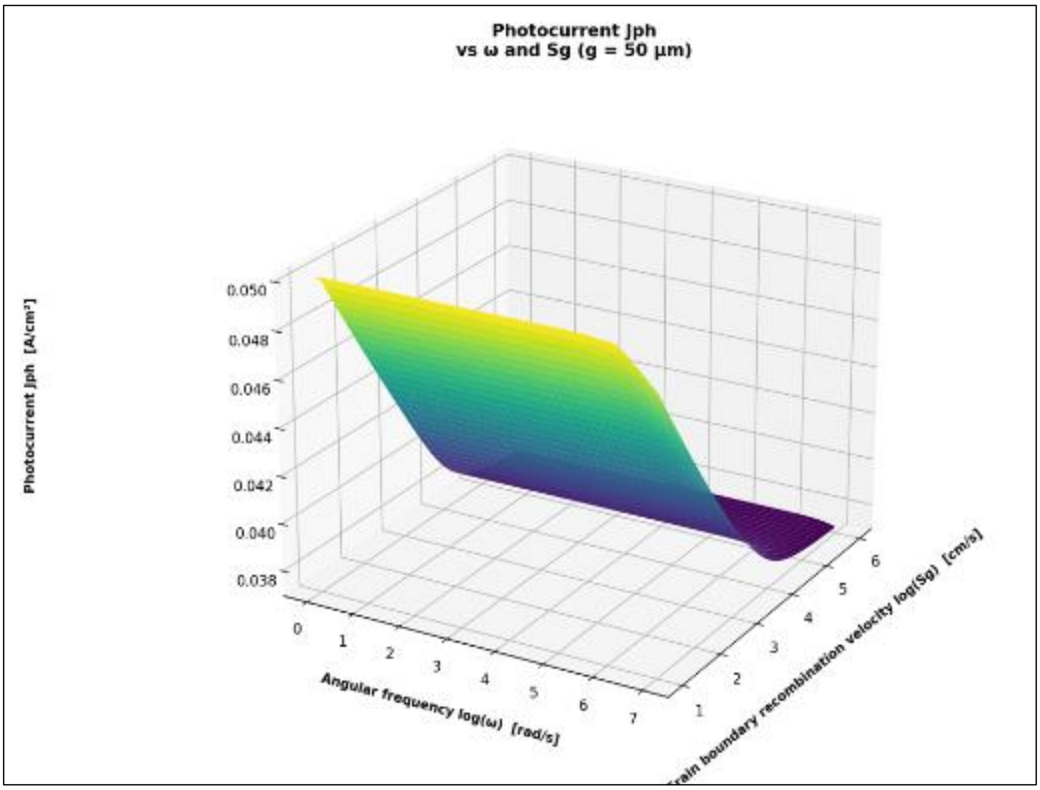

Figure 10: Photocurrent Jph as a function of the angular frequency ω and the grain-boundary recombination velocity Sg (g = 50 µm).

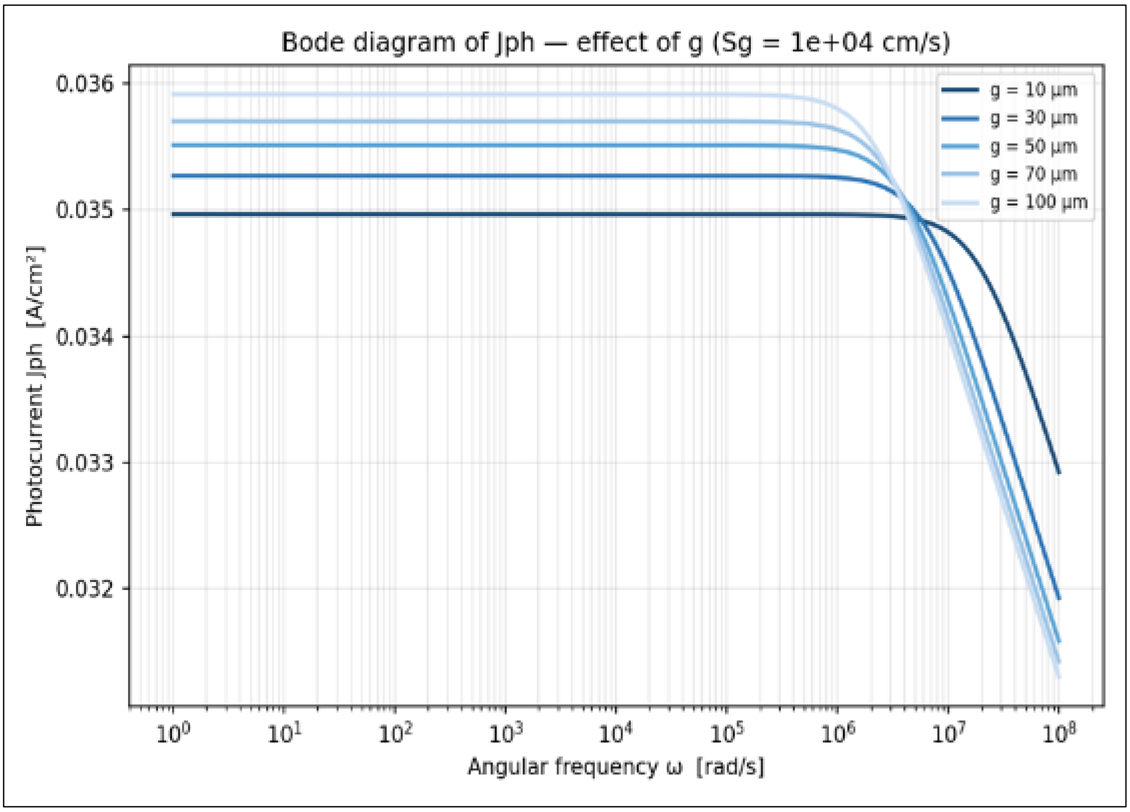

Figure 11: Bode diagram of the photocurrent Jph — effect of grain size g (Sg = 10^4 cm/s).

The photocurrent, calibrated to remain within the physical range 0.03–0.05 A/cm² (Jsc ≈ 0.04 A/cm² under the reference conditions), shows a well-defined low-frequency plateau for each grain size. Beyond a cut-off frequency near 10^6–10^7 rad/s, Jph drops for all g values, consistent with the high-frequency convergence regime observed earlier for D_eff and δn.

3.4 Photovoltage Vph

Vph operates in a regime close to open-circuit conditions (low Sf) and then decreases continuously as Sf increases, as shown in the two following figures.

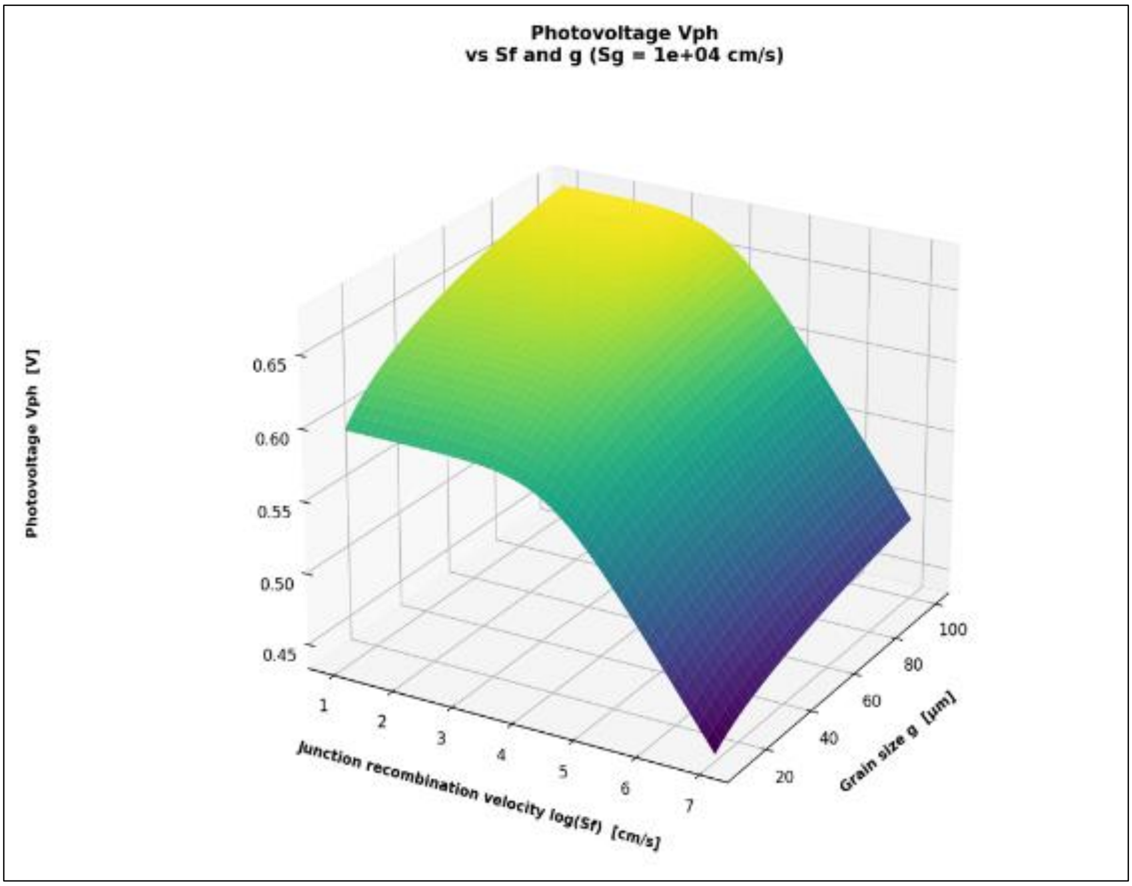

Figure 12: Photovoltage Vph as a function of the junction recombination velocity Sf and the grain size g (Sg = 10^4 cm/s).

Figure 12 shows that the effect of grain size on Vph remains moderate compared with that of Sf: over the whole range of g studied (10–100 µm), Vph varies by about 0.10 V near the open-circuit regime, whereas it varies by nearly 0.20 V as Sf spans its full range of values, thus confirming that the collection conditions at the junction dominate the behaviour of the photovoltage.

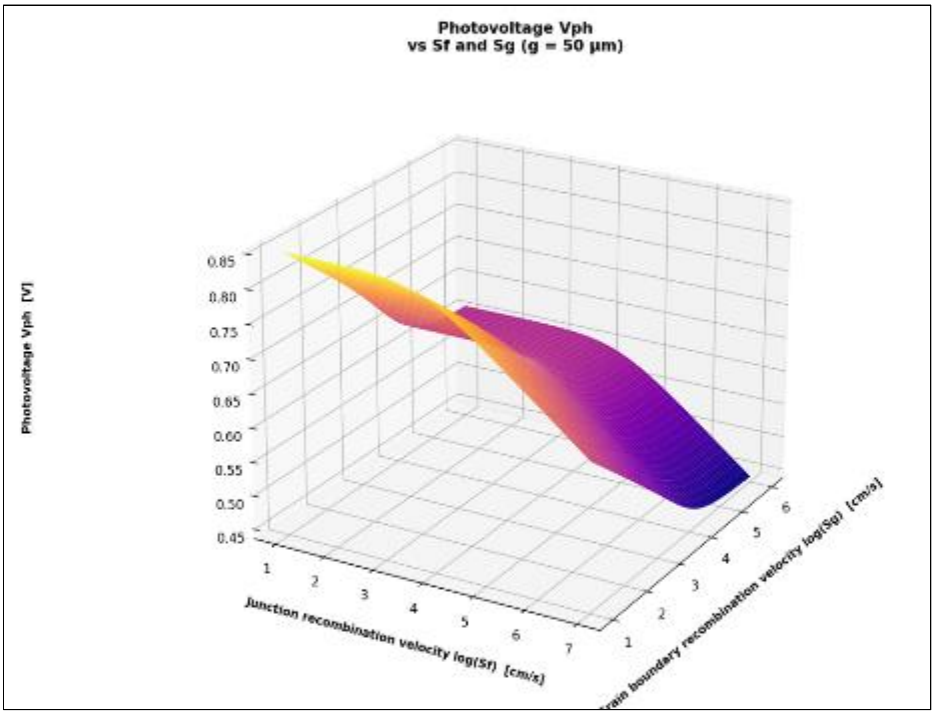

Figure 13: Photovoltage Vph as a function of the junction recombination velocity Sf and the grain-boundary recombination velocity Sg (g = 50 µm).

Figure 13 illustrates the effect of Sg at fixed grain size: Vph decreases appreciably as Sg increases, consistent with a reduction of the carrier density available for accumulation at the junction, due to more intense grain-boundary recombination.

3.5 Synthesis: Jsc, Voc and D_eff

Table 1: The values of the short-circuit photocurrent (Jsc, at Sf → 10^7 cm/s), the open-circuit voltage (Voc, at Sf → 10 cm/s) and the static effective diffusion coefficient (D_eff, at ω = 0) for six representative combinations of (g, Sg).

Combination	Jsc [A/cm^2]	Voc [V]	D_eff [cm^2/s]
g=10µm, Sg=10^4	0.0394	0.596	1.364
g=50µm, Sg=10^4 (reference)	0.0389	0.650	6.705
g=100µm, Sg=10^4	0.0389	0.677	12.177
g=50µm, Sg=10^2	0.0462	0.788	25.017
g=50µm, Sg=10^5	0.0376	0.615	2.854
g=50µm, Sg=10^6	0.0374	0.609	2.437

This table reveals a remarkable consistency among the three quantities: the most favourable combination in D_eff (g = 50 µm, Sg = 10^2 cm/s, D_eff = 25.0 cm^2/s, close to the intrinsic value D = 26 cm^2/s) is also the one with the highest Voc (0.788 V), a near-ideal junction only weakly limiting transport and favouring carrier accumulation at the junction. Conversely, Jsc varies relatively little across the whole table (0.037–0.046 A/cm^2, a factor smaller than 1.25), whereas D_eff varies by a factor greater than 10 (2.4 to 25.0 cm^2/s) over the same set of combinations: the short-circuit current, computed under conditions where the junction already collects most of the generated carriers efficiently, is markedly less sensitive to the quality of base transport than D_eff and Voc, which reflect the microstructural state more directly.

4 CONCLUSION

This work has established a coherent set of four transport parameters (effective diffusion coefficient, density, photocurrent and photovoltage) characterising a parallel vertical-junction polycrystalline silicon solar cell, considering the combined effects of the modulation frequency, the grain-boundary recombination velocity and the grain size. The results consistently show that an increase in the grain-boundary recombination velocity (Sg) or a decrease in the grain size (g) degrades all of these parameters.

The most striking result is the identification of a high-frequency convergence regime (beyond $\omega \approx 10^6$ rad/s) common to the four quantities studied: whatever the intensity of grain-boundary recombination or the grain size, all curves converge toward the value characteristic of the single-crystal material. This result opens an interesting perspective: high-frequency dynamic operation could serve as a strategy to partially overcome the limitations linked to the microstructural quality of the polycrystalline material.

A direct comparison of Jsc, Voc and D_eff (Table 1) reveals a second original result: although derived from the same model and sensitive to the same microstructural parameters, these three quantities do not respond with the same amplitude to a degradation of Sg or g. D_eff and Voc vary by a factor greater than 10, which makes them reliable indicators of microstructural quality, whereas Jsc (the most functional parameter measured during experimental characterisation) varies by a factor smaller than 1.25 over the same range. This observation suggests not relying solely on the short-circuit current to assess the quality of a polycrystalline solar cell; combined measurements including the open-circuit voltage and, where possible, a frequency-domain characterisation of minority-carrier transport should rather be preferred.

STATEMENTS ON COMPLIANCE WITH ETHICAL STANDARDS

Acknowledgments

The authors gratefully acknowledge the late Professor Grégoire Sissoko, Full Professor (Professeur Titulaire) at the Department of Physics, Faculty of Sciences and Techniques, Cheikh Anta Diop University (UCAD), Dakar, who introduced the corresponding author to scientific research and supervised his doctoral thesis; this work is dedicated to his memory.

Disclosure of conflict of interest

The author declares no competing interests

Author contributions

M. S. Diouf designed the study, developed the model, performed the calculations and prepared the figures. O. Mballo and A. Thiam contributed to the analysis and interpretation of the results and to the revision of the manuscript. All authors read and approved the final version.

Data availability

The data supporting the findings of this study, together with the numerical worksheets used to generate the figures, are available from the author on reasonable request.

REFERENCES

[1] J.Y.W. Seto, The electrical properties of polycrystalline silicon films, Journal of Applied Physics, 46, (1975), pp. 5247-5254. https://doi.org/10.1063/1.321593

[2] H.C. Card, E.S. Yang, Electronic processes at grain boundaries in polycrystalline semiconductors under optical illumination, IEEE Transactions on Electron Devices, 24, (1977), pp. 397-402. DOI: 10.1109/T-ED.1977.18747

[3] J.D. Zook, Effects of grain boundaries in polycrystalline solar cells, Applied Physics Letters, 37, (1980), pp. 223-226. https://doi.org/10.1063/1.91832

[4] M. Boiro, B. Dione, I. Toure, A. Ndiaye, A. Diao, Influence of the Magnetic Field on the Diffusion Capacitance of a Serial Vertical Junction Silicon Solar Cell in Frequency Modulation, American Journal of Modern Physics, 11(1), (2022), pp. 1-6.

[5] Gökhan Şahin, Sabir Rüstemli, Influence of Base Depth on the Frequency-Dependent Impedance Characteristics of Vertical Silicon Solar Cells Using Dynamic Impedance Spectroscopy, International Journal of Energy Research, 2026, Article 7618204.https://doi.org/10.1155/er/7618204

[6] M.B. Sene, A. Diao, A. Faye, C. Mbow, 3-D Modeling of a Polycrystalline Silicon Solar Cell Under Polychromatic Illumination: Effects of the Grain Size and the Recombination Velocity at the Boundaries, American Journal of Modern Physics, 10(3), (2021), pp. 55-59.https://doi.org/10.11648/j.ajmp.20211003.13

[7] A. Dieng, I. Zerbo, M. Wade, A.S. Maiga, G. Sissoko, Three-Dimensional Study of a Polycrystalline Silicon Solar Cell: The Influence of the Applied Magnetic Field on the Electrical Parameters, Semiconductor Science and Technology, 26 (2011) 095023. https://doi.org/10.1088/0268-1242/26/9/095023

[8] I. Ouedraogo, et al., Investigation of the Polycrystalline Silicon PV Cell Efficiency in 3D Approximation versus Electromagnetic Field under Monochromatic Illumination, International Journal of Photoenergy, 2021 (2021) 5171351. https://doi.org/10.1155/2021/5171351

[9] A. Diao, N. Thiam, M. Zoungrana, G. Sahin, M. Ndiaye, G. Sissoko, Diffusion Coefficient in Silicon Solar Cell with Applied Magnetic Field and under Frequency: Electric Equivalent Circuits, World Journal of Condensed Matter Physics, 4 (2014) 84–92. https://doi.org/10.4236/wjcmp.2014.42013

[10] D. Faye, B. Dione, M. Boiro, P. Diop, Determination of the Series Resistance of a Series Vertical-Junction Silicon (N+/P/P+) Solar Cell under Polychromatic Illumination and Magnetic Field: Effect of Optimum Thickness, Journal of Modern Physics, 15 (2024) 1543–1554. https://doi.org/10.4236/jmp.2024.1510064

[11] M. Khalis, R. Masrour, Predominant Range of Serial Resistance and Recombination Velocity at Different Concentration Levels: Vertical Multijunction Cell, Silicon, 14 (2021) 6107–6112. https://doi.org/10.1007/s12633-021-01374-z

[12] N.D. Arora, J.R. Hauser, D.J. Roulston, Electron and Hole Mobilities in Silicon as a Function of Concentration and Temperature, IEEE Transactions on Electron Devices, 29 (1982) 292–295. https://doi.org/10.1109/T-ED.1982.20698

[13] J. Furlan, S. Amon, Approximation of the Carrier Generation Rate in Illuminated Silicon, Solid-State Electronics, 28 (1985) 1241–1243. https://doi.org/10.1016/0038-1101(85)90048-6